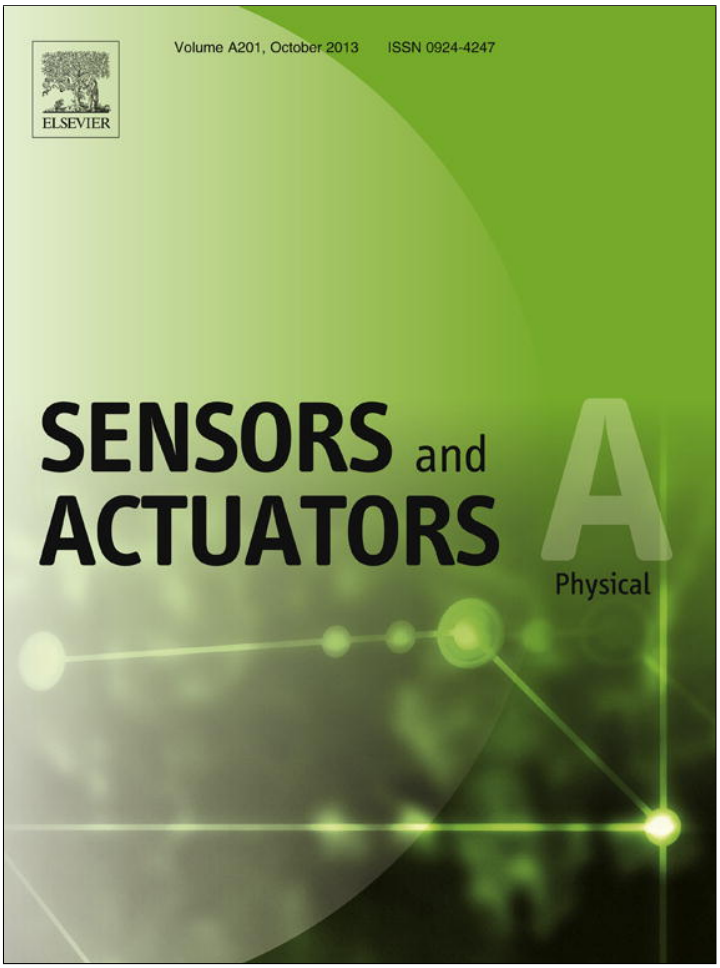

Sensors and Actuators A 201 (2013) 1–9

Contents lists available at ScienceDirect

Sensors and Actuators A: Physical

journal homepage: www.elsevier.com/locate/sna

Development of a lead-zirconate-titanate (PZT) thin-film microactuator probe for intracochlear applications

Chuan Luo [a], G.Z. Cao [b], I.Y. Shen [a,*]

[a] Department of Mechanical Engineering, University of Washington, Seattle, WA 98195-2600, USA
[b] Department of Material Science & Engineering, University of Washington, Seattle, WA 98195-2120, USA

ARTICLE INFO

Article history:
Received 28 February 2013
Received in revised form 27 June 2013
Accepted 30 June 2013
Available online 8 July 2013

Keywords:
PZT thin film
PZT probe
Microactuator
Intracochlear applications
Parylene package
Acoustic stimulation
Impedance

ABSTRACT

In this paper, we present design, fabrication, and testing results of a small-scale piezoelectric lead-zirconate-titanate (PZT) thin-film microactuator probe that could be implanted in the inner ear for hearing rehabilitation. The PZT probe would generate a pressure wave directly stimulating perilymph in the cochlea to provide acoustic stimulation. Specifically, the PZT probe is 1-mm wide, 10-mm long, and 0.4-mm thick with a PZT thin-film diaphragm at the tip of the probe serving as an acoustic actuator. The diaphragm size is 0.8 mm × 0.8 mm and the probe is packaged with parylene of 0.25-μm thickness. The design effort includes finite element simulations to determine thickness of the parylene package as well as back-of-the-envelope calculations of implantation depth of the PZT probe. The fabrication work includes deposition of a PZT thin film via sol–gel processes, deep reaction ion etching to form an array of vibrating PZT diaphragms, dicing the wafer to release the PZT probes, and application of parylene layer to package the PZT probes. The testing effort includes measurements of actuator velocity (via a laser Doppler vibrometer) and impedance (via an impedance analyzer) in air and in water. After the PZT probe is submerged in water, its displacement gradually increases and saturates at around 2 h. Impedance measurements also show a similar trend. To explain these phenomena, we hypothesize that water infiltrates into the PZT thin film via diffusion, thus increasing the dielectric constant of the PZT film. SEM images reveal numerous nano-pores on PZT and probe surfaces, indirectly supporting the hypothesis. The PZT probe functions in water for 55 h without breaking down.

1. Introduction

Hearing loss is a common disability in aging seniors and people who work long hours in noisy environments. The majority of persons with hearing loss have sensori-neural impairments, due to dysfunction or loss of cochlear hair cells. For people with mild to moderate hearing loss, conventional hearing aids can amplify the sound level and provide a significant degree of rehabilitation. For moderately severe to profound hearing loss (e.g., nearly deaf), patients may undergo surgical placement of a cochlear implant that stimulates the auditory nerve electrically. Many individuals, however, retain only low-frequency hearing. Traditional hearing aids are often marginally effective for these patients. Moreover, these patients have not been candidates for standard cochlear implants either, because there is a risk to damage the low-frequency hearing in surgery [1].

Recently, there is evidence that the most effective type of rehabilitation for this growing cadre of patients is to combine electrical and acoustic stimulation (CEAS) in the same ear [1–3]. The basic idea is to use a cochlear implant with a shortened electrode to electrically stimulate the high-frequency region (i.e., electric stimulation). A traditional hearing aid is then used to amplify the acoustic signal delivered to the low-frequency region (i.e., acoustic stimulation). A future strategy for CEAS is to replace the traditional hearing aid with an intracochlear acoustic actuator, which generates pressure waves in the cochlea serving as the acoustic stimulation [4,5]. The intracochlear acoustic actuator can be integrated with a shortened electrode to form a hybrid cochlear implant (Fig. 1) leading to a single and totally implantable device.

Despite its novelty, a major obstacle has been the availability of an acceptable intracochlear acoustic actuator. The size of cochlea is about the size of a pea. The actuator can have a maximal cross section of about 1 mm to be potentially implanted in cochlea. The intracochlear actuator must have large enough displacement and acoustic impedance to move perilymph fluid inside cochlea to generate pressure waves. Also, the intracochlear actuator must be properly packaged to function in the aqueous environment in cochlea.

To prove the concept of this strategy, the authors have been developing intracochlear microactuators using Lead-Zirconate-Titanate (PZT) thin films since 2004 [6–9]. The development efforts include conceptual design, fabrication, prototyping, testing, and

* Corresponding author. Tel.: +1 206 543 5718; fax: +1 206 685 8047.
E-mail address: ishen@u.washington.edu (I.Y. Shen).

0924-4247/$ – see front matter © 2013 Elsevier B.V. All rights reserved.
http://dx.doi.org/10.1016/j.sna.2013.06.027

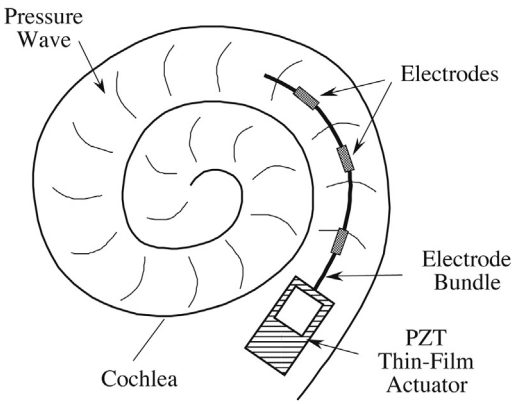

Fig. 1. Conceptual design of a hybrid cochlear implant.

numerical simulations. The microactuators take the form of a membrane structure consisting of four parts: a silicon diaphragm, a bulk silicon substrate, a PZT thin film layer, and a pair of electrodes; see Fig. 2. (Note that the parts in Fig. 2 are not drawn in proportion.) The silicon diaphragm is a moving component of the actuator anchored to the silicon substrate. As a result of its small thickness, the silicon diaphragm has low structural stiffness compared with the substrate. On top of the silicon diaphragm is a layer of PZT thin film with a pair of bottom and top electrodes. When a driving voltage is applied to the electrodes, the PZT thin film extends or contracts in the plane of the diaphragm, thus creating a bending moment to flex the diaphragm out of its plane. Such PZT thin-film membrane actuators have appeared in many MEMS applications including micro fluidic devices (pumps, valves and nozzles) [10–14], micro optic scanners [15–19], micro-deformable mirrors [20–22], micro high fidelity speakers [23,24], micro bio-device [25–27], micro ultrasonic device [28,29], micro gyroscope [30], and fuel cell membrane [13]. Similarly, the diaphragm structure is widely used in various transducers, such as micro energy generators [31–33], micro energy harvesters [34,33,35], micro mass sensors [36,37], micro pressure sensors [38], and micro distance sensor [39].

Nonetheless, transition from an actuator platform in Fig. 2 to an actual probe that can be potentially implantable is not trivial. Many challenges need to be overcome. The first challenge is structural rigidity. The past development efforts on PZT microactuators in [6–9] are all at the wafer level. Therefore, all four edges of the PZT diaphragm are rigidly anchored in the wafer. When the diaphragm is diced off the wafer, its anchor is significantly weakened. As a result, natural frequencies of the microactuator drop and frequency bandwidth is reduced. Moreover, the microactuator needs to be packaged in order to function in the aqueous environment in cochlea. Therefore, the presence of packaging materials will increase the thickness of the diaphragm reducing the actuator displacement. Therefore, a thorough analysis is needed to design the amount of anchor, a proper implantation depth, and the thickness of the packaging materials.

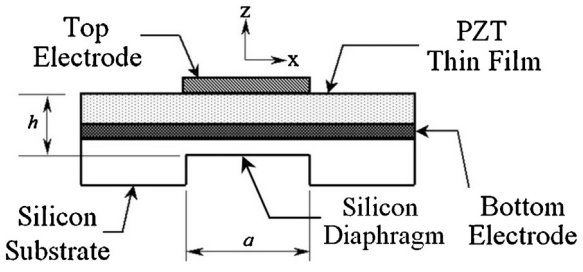

Fig. 2. Schematic drawing of a PZT thin-film microactuator (not to scale).

The second challenge is fabrication—in particular a novel release mechanism that dices the PZT probes off the wafer in large quantities. Poor selection of the release mechanism will not only significantly reduce the yield of the final PZT probes, but also make the fabrication process very inefficient. After the PZT probes are released, they need to be tested for quality assurance first, then packaged by parylene, and finally tested again. Therefore, it becomes critical to design a novel fixture that handles the diced PZT probes effectively, so that the subsequent fabrication process can be streamlined.

The third challenge is testing. Since the probes will be used to generate pressure waves in intracochlear perilymph fluid, the probes need to be tested in an aqueous environment to ensure their performance before they are implanted. For example, the probes shall not become shorted during an acute animal test, the probes shall generate enough displacement in the aqueous environment, and so on.

The purpose of this paper is to report how we overcome these challenges to develop a PZT thin-film microactuator probe that could be potentially implanted in cochlea for acute animal tests. For the rest of the paper, we will first demonstrate a conceptual design of a PZT probe that can be implanted in cochlea to generate acoustic pressure waves. Then we conduct a finite element analysis to design key parameters of the probe, such as implantation depth and the thickness of parylene package. The next step is to fabricate the probes. In this step, we will address the key challenges discussed above, including the release mechanism and fixture design. Finally, we will present experimental results, while the probe is tested in air and in water, to demonstrate the probe's performance. We conduct the experiments by measuring frequency response functions (FRFs) and impedance to ensure that the measurements are consistent. New phenomena are observed and hypotheses are made to explain these new phenomena.

2. Conceptual design

Fig. 3 illustrates a conceptual design of the PZT thin-film microactuator probe. The dimensions of the probe are 1 mm wide, 10 mm long, and 0.4 mm thick. At the tip of the probe, there is a PZT diaphragm serving as an acoustic actuator. The PZT diaphragm has the same design as shown in Fig. 2 with a size of 0.8 mm by 0.8 mm, while the thickness h of the diaphragm is roughly 2 to 3 μm. This leads to a thin-wall structure anchoring three sides of the PZT diaphragm, with the thickness of the thin walls being 100 μm and the height being 400 μm; see the backside of the probe in Fig. 3. We will verify via experiments if the thin walls are strong enough to anchor the PZT diaphragm without losing its frequency bandwidth.

To boost the actuator displacement, we use dual top electrodes shown in Fig. 4 instead. When the diaphragm deforms, the central portion and the outer portion of the diaphragm always have opposite curvatures. For example, if the diaphragm experiences an upward displacement, the central portion is concave downward and the other portion is concave upward. When the two electrodes are driven in an out-of-phase manner, the actuator displacement can be increased by a margin of 30% [9].

The PZT actuator probes also have lead wires for bottom and top electrodes of the PZT diaphragm. The entire actuator is packaged with parylene of no more than 2-μm thick. The proper thickness will be determined via a finite element analysis.

For the target intracochlear application, the tip of the PZT microactuator probe—roughly the first 1–1.5 mm—will be implanted inside the basilar region of cochlea. (The length of the implanted portion will be referred as "implantation depth" for the rest of the paper.) After the tip of the PZT probe is implanted in cochlea, the probe will be anchored to skull bone. The tip portion

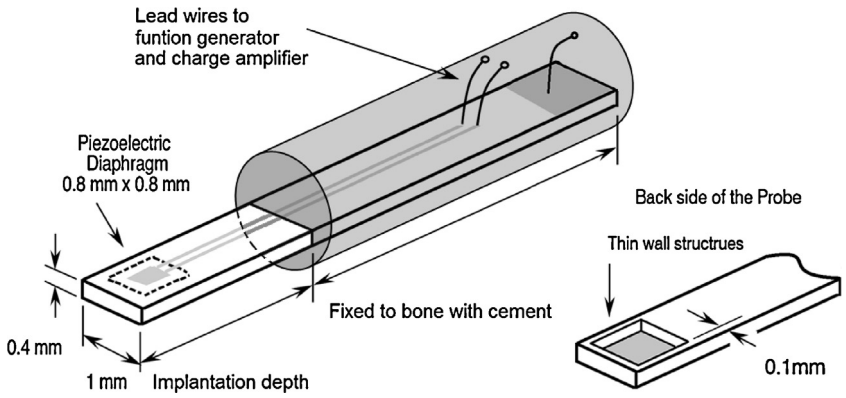

Fig. 3. Conceptual design of a PZT thin-film microactuator probe.

of the probe will then form a cantilever beam inside cochlea, while the remaining part of the actuator probe will be outside the skull to accommodate lead wires for power and measurement electronics; see Fig. 3. In order not to degrade the probe's performance, the target implantation depth will be confirmed by theoretical analyses and experimental measurements.

3. Theoretical analyses

The theoretical analyses have two objectives to achieve. The first objective is to estimate how much the packaging materials will reduce the actuator displacement. This will be achieved via a finite element analysis. The second objective is to estimate how much the implantation depth will affect the actuator bandwidth. This will be achieved via a back-of-the-envelope calculation.

3.1. Actuator displacement

We modify the finite element model in [9] to estimate how much parylene package reduces the actuator displacement. Since the finite element model has been described in detail in [9], it is not repeated here to save space. The modification includes a layer of parylene added on the top surface covering the PZT diaphragm, top electrodes, and the anchor; see Fig. 5. Additionally, a second layer of parylene is added to the bottom of the diaphragm portion of the actuator. Since parylene deposition used in the probe fabrication is conformal, both layers will be deposited at the same time. Therefore, the thicknesses of the two layers are identical and must be varied simultaneously in the finite element model. Material properties of parylene (N-type) used in the finite element analysis include density (1.11 g/cm^3), Young's modulus (2.4 GPa), and Poisson's ratio (0.4).

Fig. 6 shows how thickness of the parylene layer affects actuator displacement in percentage. The actuator displacement is normalized with that of a reference actuator with no parylene package. In addition the thickness of the reference PZT diaphragm portion is 2.22 μm thick. According to Fig. 6, a 2-μm thick parylene package will reduce the actuator displacement by 30%.

3.2. Actuator bandwidth

The frequency bandwidth of the PZT actuator probe will be limited by the lowest natural frequency of the probe. When the PZT diaphragm is located in a wafer, its four edges are rigidly anchored.

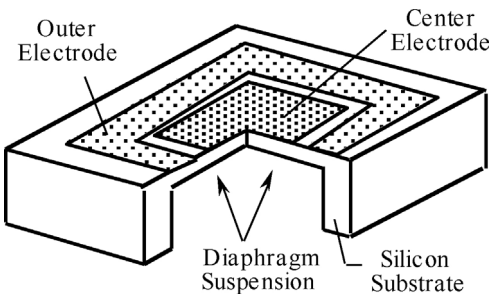

Fig. 4. Schematic drawing of a dual top electrode design.

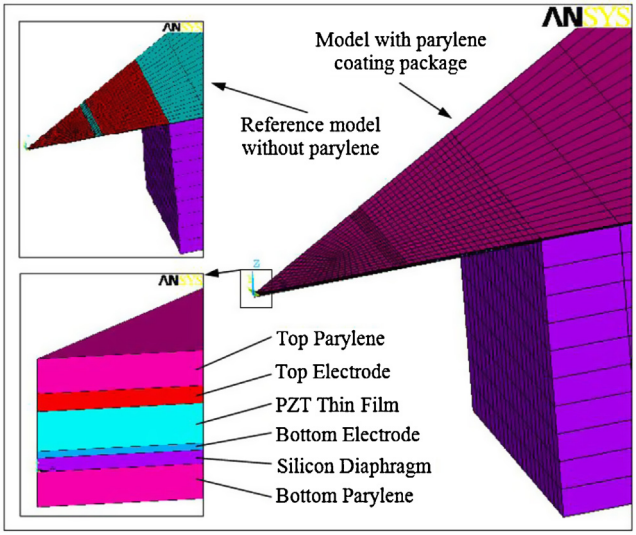

Fig. 5. Finite element model of PZT actuator with parylene coating package.

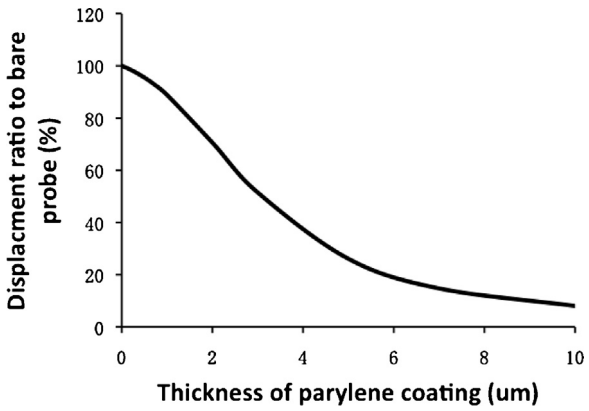

Fig. 6. Reduction of actuator displacement as a function of parylene thickness.

Table 1
Upper and lower bounds of the first natural frequency.

Probe length L_{max} (mm)	L_{min} (mm)	b_{max} (mm)	b_{min} (mm)	Lower bound f_{min} (kHz)	Upper bound f_{max} (kHz)	Exp. results (kHz)
12.2	11.30	2.279	1	3.11	5.56	4.30
10.5	9.60	2.101	1	4.32	7.60	6.70
5.95	5.05	1.524	1	14.58	26.25	19.80
2.0	1.10	1.210	1	140	520	N/A

As a result, its first natural frequency solely comes from the vibration of the diaphragm. In the PZT probe shown in Fig. 3, however, the three thin-wall edges give much less anchor compared with the fourth edge. As the PZT diaphragm vibrates, it will distort the thin walls significantly more than the fourth edge. In other words, the PZT diaphragm is no longer fixed at its four edges. Therefore, actuation of the PZT diaphragm will cause local deformation that behaves like an end moment exciting the PZT probe as a cantilever.

When the PZT probe is implanted in cochlea, the probe will be anchored to skull bone forming a cantilever beam; see Fig. 3. Therefore, the depth of the implantation will determine the length of the PZT probe in cochlea. If the length is too large, the natural frequency could drop significantly thus reducing the bandwidth of the PZT probe. Therefore, it is important to determine the length of the PZT probe, or implantation depth, to ensure enough frequency bandwidth.

To expedite the fabrication, the final PZT probes will have a trapezoidal shape as shown in Fig. 7 (detailed reasons to be explained in the next section). The total length of the probe is L_{max} and the non-diaphragm portion has length L_{min}. The shortest width b_{min} occurs at the probe tip with the diaphragm (i.e., the free end), and the largest width b_{max} occurs at the base of the beam (i.e., the cantilevered end). Since we only need a rough estimate of the first natural frequency, it will be an overkill to employ a full-blown finite element analysis. Alternatively, we perform a back-of-the-envelope calculation using the following textbook formula to estimate the first natural frequency of a uniform fixed-free cantilevered beam with a rectangular cross section

$$f_1 = \frac{1}{2\pi}\left(\frac{1.875}{L}\right)^2\sqrt{\frac{EI}{m}} \quad (1)$$

In Eq. (1), f_1 is the first natural frequency in Hz, L is the length of the beam, E is the Young's modulus, and m is the mass per unit length of the beam. Also in Eq. (1), $I = (bh^3/12)$ is the area moment of inertia of the beam section, where b and h are the width and height (thickness) of the beam, respectively.

Since the PZT probe is not uniform and the probe tip has a diaphragm structure, Eq. (1) can only be used to estimate an upper and a lower bound of the first natural frequency. The upper bound will occur when $L = L_{min}$ and $b = b_{max}$. Similarly, the lower bound will occur when $L = L_{max}$ and $b = b_{min}$. Table 1 lists the upper and lower bounds for different length L. As shown in Table 1, when the probe length is down to 5.9 mm, the first natural frequency of the probe will be at least 14 kHz. If only the first 2 mm of the probe is implanted, the natural frequency of the beam will be more than 100 kHz, which has exceeded the audible frequency range (20 Hz–20 kHz). In that case, the vibration of the PZT diaphragm will dominate. Therefore, as long as the implantation depth is less than 5.9 mm, the PZT probe should have enough a bandwidth for intracochlear applications focusing on low end of the audible frequency range.

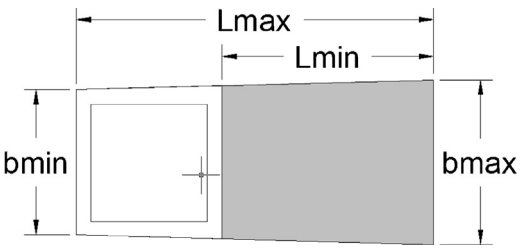

Fig. 7. Actuator shape used in the back-of-the envelope calculation for natural frequencies.

4. Fabrication of PZT probes

We adopt a radial layout to fabricate the PZT probes, see Fig. 8. Each probe extends radially with the PZT diaphragm pointing to the center. The radial layout has several advantages. First, the PZT diaphragm will have fairly uniform quality, because the radial layout ensures that each probe has an equal distance from the PZT diaphragm to the center of the wafer. Since spin coating is used in depositing the PZT thin film, the equal distance implies equal thickness of deposited PZT film at the diaphragm area. The radial layout also results in a larger area at the cantilevered end of the probes making interconnects a less challenging task.

Fig. 9 illustrates the fabrication process using an improved sol–gel process that employs rapid thermal annealing and a dilute sealant coating. The silicon substrate is first oxidized in a furnace

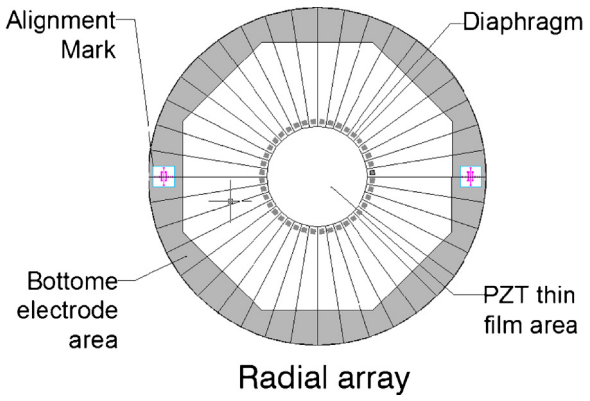

Fig. 8. Layout of the PZT probes.

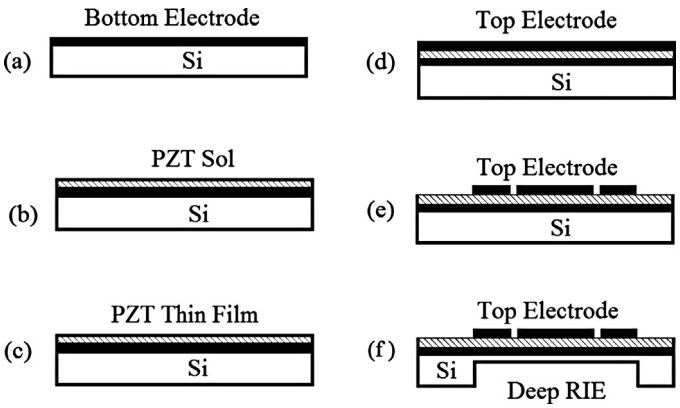

Fig. 9. Fabrication processes of PZT thin-film probes.

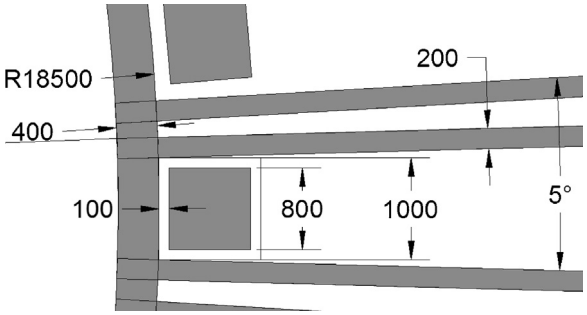

Fig. 10. Blowup view of the mask used in DRIE (units: μm).

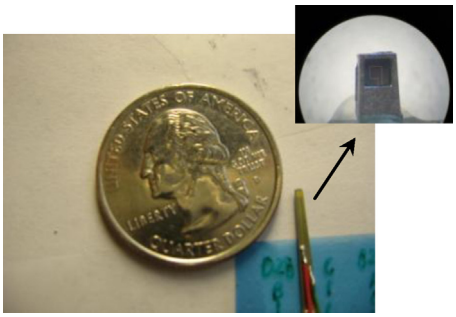

Fig. 11. Photo of a fabricated PZT thin-film microactuator probe.

at 1045 °C for 2 h to grow a SiO_2 layer of 500 nm thick. Then a layer silicon nitride of 200 nm thick is deposited by PECVD (plasma enhanced chemical vapor deposition). The bottom electrode consists of Pt/Ti layers with thickness of 100 nm and 50 nm, respectively (Fig. 9(a)). The PZT film is spin-coated three times. For the first two coatings, the sintering temperature is 650 °C for 15 min. For the third coating, the sol is diluted 50% by acetic acid and sintering temperature is 450 °C for 10 min (Fig. 9(b) and (c)). The top electrode layer consists of Au/Cr layers through evaporation (Fig. 9(d)). The top electrode layer is then patterned to form the center and outer electrodes (Fig. 9(e)). Finally, the backside of the silicon is etched via deep reactive ion etch (DRIE) to form the diaphragm suspension (Fig. 9(f)). The thickness of the PZT film is measured around 1 μm. Please note that the schematic drawings in Fig. 9 mainly illustrate the fabrication process of the PZT probes (e.g., electrodes and diaphragms). Mechanisms to release the PZT probes from the wafer are not included in Fig. 9 and will be discussed later in detail.

Now let us explain how the fabrication process in Fig. 9 works in the context of the radial layout in Fig. 8. First of all, a bottom electrode is deposited over the entire wafer (cf. Fig. 9(a)). Then the gray area along the perimeter in Fig. 8 is shielded with blue tapes. Next, PZT thin film is deposited using spin coating (cf. Fig. 9(b) and (c)). Since part of the bottom electrode is taped, the resulting PZT thin film will only appear over the white, octagonal area of Fig. 8. Top electrodes are then fabricated onto the PZT thin film (cf. Fig. 9(d) and (e)). (Note that the top electrodes are not explicitly shown in Fig. 8.) Finally, DRIE is used to form the PZT diaphragms (cf. Fig. 9(f)), which appear as tiny dark squares in Fig. 8.

The PZT probes are simultaneously released from the wafer during the step of DRIE. Fig. 10 shows a blowup view of the mask used in DRIE. The gray area is the etch-away portion by DRIE, and the white portion defines the resulting PZT probes. The etch-away portion includes two parts. The first part is the square diaphragms, which have already been explained extensively in Figs. 8 and 9(f). The second part is release slots that are either radial or circular in shape locating around each PZT probe. (These release slots also appear as dark radial lines and circle in Fig. 8.) They are explained in detail as follows.

These release slots around each PZT probe are very critical. At the end of DRIE, not only are the PZT diaphragms formed but also these slots that gently support the PZT probes. At this time, the PZT probes can be easily released from the wafer by breaking these slots. In order to break these slots easily, the width of the slots needs to exceed a critical value. After a few trials and errors, we find that a slot width of at least 200 μm is needed. Fig. 11 shows photos of a released PZT probe. In general, the thickness of the PZT probe is 400 μm, while the thickness h of the diaphragm is roughly 2–3 μm as designed in Fig. 3.

After the probes are released, they are placed in a special fixture and secured via Silicone; see Fig. 12. The released probes have different protrusion portions in the fixture to mimic the implantation

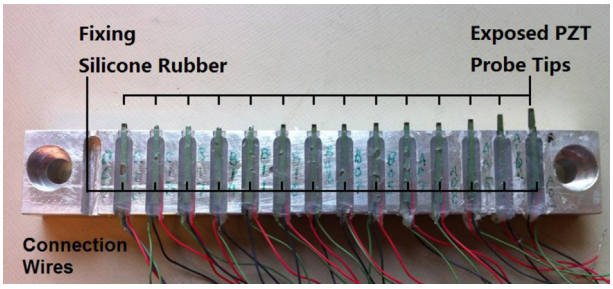

Fig. 12. Fixture holding released probes for parylene packaging.

depths. The fixture and the probes are then packaged with conformal parylene coating. Fig. 13 shows cross sectional view of a PZT probe at the diaphragm area. The thickness of the parylene coating is 0.25 μm. Based on the calculation in Fig. 6, the 0.25-μm thick parylene will reduce actuator displacement no more than 5%. After the packaging, the PZT probes along with the Silicone can be easily released from the fixture for testing.

5. Experimental measurements

After the PZT probes are packaged, they are tested in air and in water. These tests and their results are explained in detail as follows.

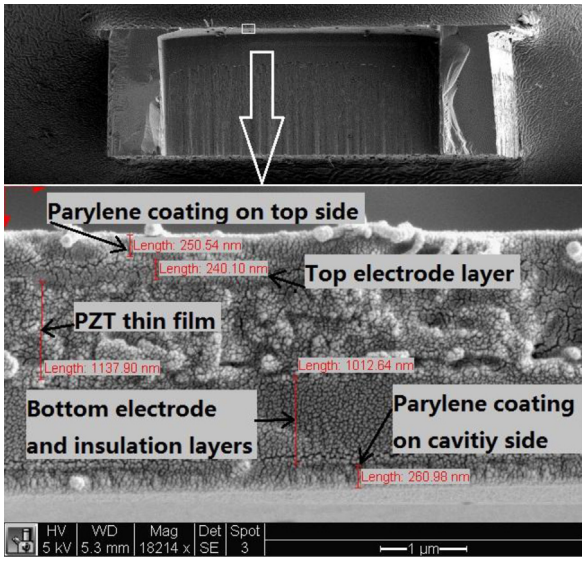

Fig. 13. Cross sectional views of the PZT diaphragm packaged with parylene.

Table 2
Displacement and natural frequency of PZT probes before and after parylene package is coated.

Device	Displacement			Natural frequency		
	Before coating (nm/V)	After coating (nm/V)	Variation (%)	Before coating (kHz)	After coating (kHz)	Variation (%)
1	10.18	9.95	97.74	59.79	58.19	97.34
2	11.38	11.32	99.47	58.82	57.75	98.18
3	12.65	12.50	98.81	56.91	54.87	96.42
4	14.73	14.45	98.10	58.38	56.42	96.64

5.1. Tests in air

The purpose of the tests is to establish a reference measurement of a PZT probe before it goes into a functional test in water. Specifically, the tests allow us to identify proper implantation depth and boundary conditions to maintain the bandwidth of the PZT probe (cf. Section 3.2).

Fig. 14 shows a PZT probe and its setup. The PZT probe is fixed to an aluminum block at its base via epoxy. The amount of epoxy can be added incrementally; see epoxy 1 to epoxy 4 in Fig. 14. By varying the amount of epoxy, we can control the implantation depth of the PZT probe in the experiments.

The experimental setup includes a spectrum analyzer, an AVC amplifier to drive piezoelectric load, and a laser Doppler vibrometer (LDV). A source in the spectrum analyzer generates a swept sine signal to the AVC amplifier, which subsequently drives the PZT probe. In the meantime, the LDV measures velocity of the PZT diaphragm at its center. The swept sine voltage and the LDV measurement are processed by the spectrum analyzer to generate frequency response functions (FRFs) of the PZT probe. Fig. 15 shows some measured FRFs. The measurements clearly indicate that a shorter implantation depth results in a higher natural frequency.

Table 1 also compares the measured natural frequency with the theoretical predictions using the back-of-the-envelope calculations. The comparison shows that the measured natural frequencies nicely fall within the upper and lower bounds predicted from the back-of-the-envelope calculations.

Table 2 compares the measured displacement and natural frequency of several PZT probes before and after the parylene package is coated. Experimental results show that the parylene coating reduces the displacement and the natural frequency no more than 3% and 4%, respectively.

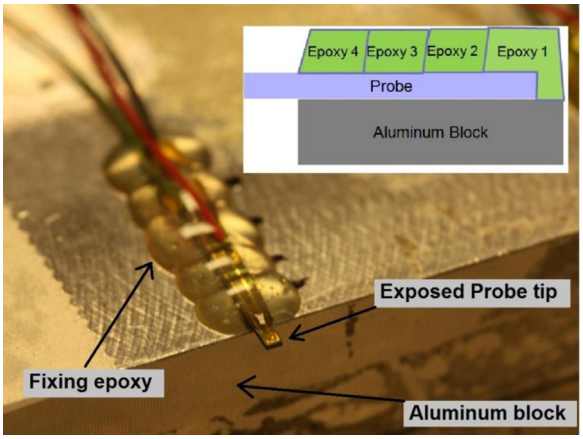

Fig. 14. A PZT probe and its experimental setup.

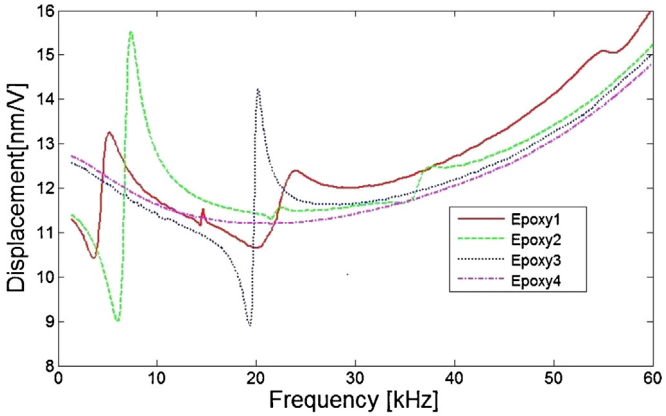

Fig. 15. Measured frequency response functions at various implantation depths.

5.2. Tests in water

Packaged and unpackaged PZT probes are submerged in deionized (DI) water for performance tests. Two types of tests are conducted. One is impedance test. Basically, one top electrode (either the center or the outer electrode) and the bottom electrodes are connected to an impedance analyzer to measure the impedance of the PZT probe. The other test is the LDV measurement described in Section 5.1. Since the LDV compares the reflected beam with a reference beam to obtain its measurement, the measured velocity will depend on the index of refraction of the medium through which the laser beam has traveled. When the test is conducted in the water, the measurements have to be divided by the index of refraction in order to obtain the true velocity of the PZT probe.

As a reference, Fig. 16 shows measured impedance (both magnitude and phase) of an unpackaged PZT probe when submerged in DI water. The impedance is measured from the center electrode to the bottom electrode. The impedance magnitude and phase measurements refer to the left and right axes, respectively. When the unpackaged PZT probe is in air, the phase is nearly 90° (−89° to be exact) indicating that the resistance is very large and the system is nearly a capacitor. When the unpackaged probe is submerged in water, the impedance magnitude drops significantly, and the phase changes to −77°, implying that the surrounding water has affected the PZT probe by substantially reducing the resistance. When the probe is taken out of the water, the impedance returns to its original

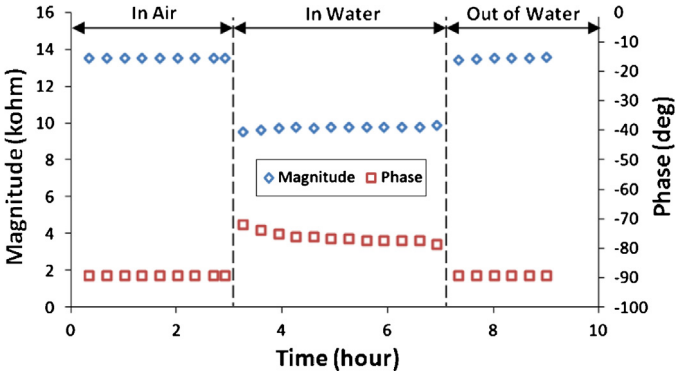

Fig. 16. Measured impedance (magnitude and phase) of an unpackaged PZT probe submerged in deionized water.

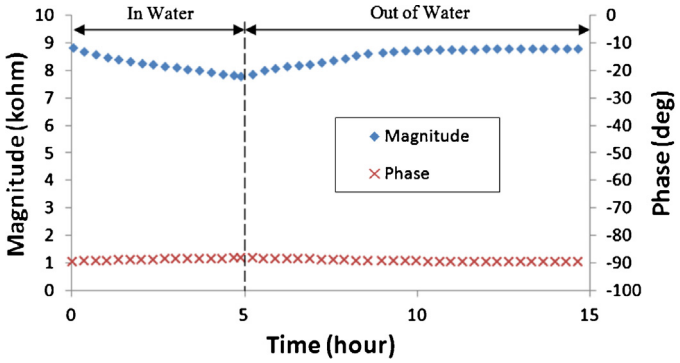

Fig. 17. Measured impedance (magnitude and phase) of a packaged PZT probe submerged in deionized water.

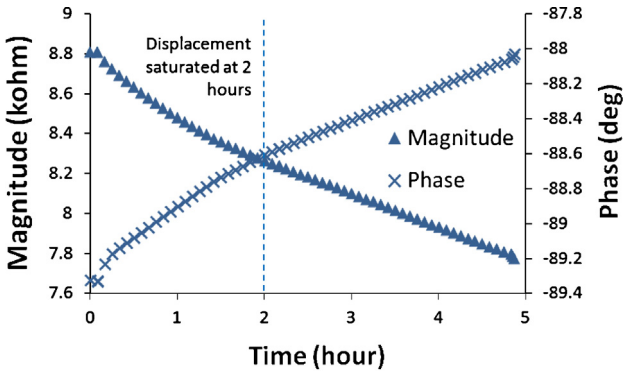

Fig. 19. Measured impedance (magnitude and phase) of a packaged PZT probe submerged in deionized water; 0–5 h.

value. Also, the change of impedance, when the probe is in and out of the water, is immediate.

In comparison, Fig. 17 shows the impedance (center to bottom electrodes) of a PZT probe packaged with parylene when submerged in and taken out of DI water. First of all, the impedance does not experience a sudden change as in the case of the unpackaged probe. Moreover, the phase of the impedance changes only slightly from −89° to −88°, even the packaged probe is in the water for 5 h. This indicates that the parylene package has protected the electrodes and the PZT thin film reasonably well and very little energy is lost to the surrounding water. The impedance magnitude, however, decreases gradually once the packaged probe is submerged in water. This indicates that the surrounding water has somehow increased the capacitance of the PZT probe.

Fig. 18 shows the measured displacement when the packaged PZT probe is submerged in the water. Specifically, the measurements come from FRFs measured via the LDV and the spectrum analyzer. The data points presented in Fig. 18 are the magnitude of FRFs at 3 kHz. Three rounds of experiments are conducted for repeatability. The first round of experiment is to test the endurance limit of the probe, so the displacement is measured at 28, 31, and 54 h. (These data are crammed into Fig. 18 for reference, denoted by the cross markers.) In the second round of the experiment, the displacement is measured more frequently (e.g., half-and-hour or 1-hour increments) after the probe is submerged in the water to 24 h. The measured displacement starts to increase from 10 nm/V as the packaged PZT probe is submerged in water, and saturates around 22 nm/V in about 2 h to a steady value. The third round of experiment focuses on the first 2 h to ensure that the measured displacement is repeatable. Experimental results show that the displacement indeed increases in the first 2 h. The blowup view in Fig. 18 shows the measured results for the first 2 h. To ensure that this displacement increase is not from thermal drift of the LDV, we conduct a separate experiment in the air for 2 h. The measured displacement remains at 10 nm/V. So the displacement increase is not from the thermal drift of the LDV.

The impedance measurements also support the observation that the displacement increases in the first 2 h. Fig. 19 shows a blowup view of the impedance measurements from the center to bottom electrodes shown in Fig. 17 for the first 5 h. Initially, the impedance magnitude drops at a faster rate, and gradually stabilizes around 2 h. Specifically, in the first 2 h, the impedance magnitude drops at a rate of 264 ohm/h. After 2 h, the impedance magnitude drops at a rate of 167 ohm/h. Something must have happened in the first 2 h in order to account for the nearly 100 ohm/h difference. This agrees with the observation that the displacement has changed in the first 2 h.

In interpreting the impedance measurements, it is more important to compare the impedance difference between two time intervals instead of the absolute measured values of the impedance for the following reason. Since the interconnects—where the impedance measurements are taken—are located at the far end from the PZT diaphragm, the PZT diaphragm and the lead wires (including the interconnects) on the probe all contribute to the measured impedance. As shown in Fig. 12, the far ends of the PZT probes are embedded in Silicone in the fixture while parylene is coated. When the PZT probes, together with the Silicone, are taken out of the fixture, certain surfaces of the Silicone are not coated with parylene. Therefore, when the entire PZT probe is submerged in a Petri dish of water, the water gradually soak into the Silicone increasing the dielectric constant of the Silicone causing the impedance to drop.

With this background information, it is obvious that the faster impedance drop in the first 2 h implies that the impedance of the PZT diaphragm has dropped in the first 2 h and eventually saturates

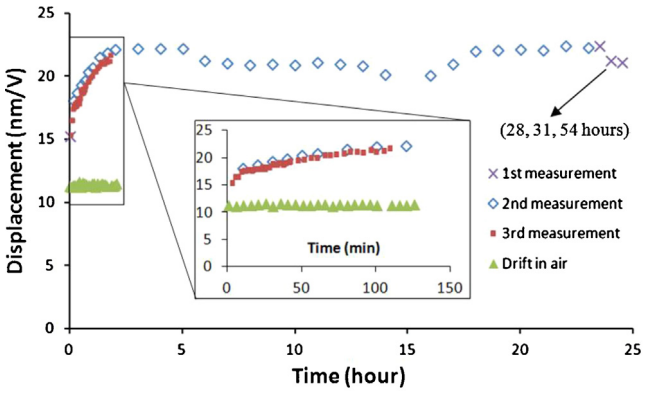

Fig. 18. Measured displacements (via LDV) of a packaged PZT probe when submerged in water.

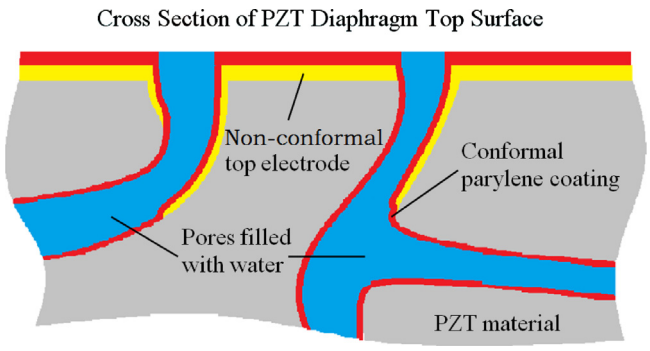

Fig. 20. Schematic drawing of the hypothesis.

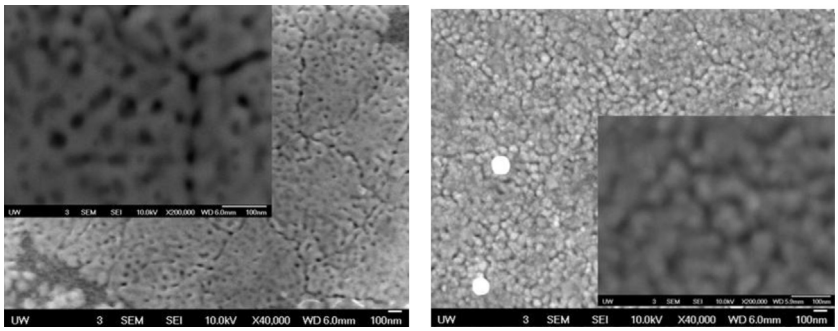

Fig. 21. High-magnification SEM images; (left) PZT surface before top electrodes are coated, and (right) PZT surface after top electrodes are deposited.

at the end of the 2 h. When the impedance of the PZT diaphragm drops, the electric current supplied to the PZT diaphragm increases. According to the constitutive equation of linear piezoelectricity, this means that the displacement has to increase. Therefore, the faster impedance drop in Fig. 19 for the first 2 h is consistent with the displacement increase in Fig. 18 for the first 2 h. The displacement increase is a real phenomenon; it is not a measurement error.

5.3. Hypothesis and evidence

It is by all means counter-intuitive that a PZT probe actually increases its displacement when it is submerged in the water. A natural question is what causes this phenomenon.

From a broader picture, there are two mechanisms that a mechanical system can increase its displacement at a frequency (e.g., 3 kHz) far lower than its natural frequency (e.g., 80 kHz). The first mechanism is that the stiffness of the system is reduced. This is rather unlikely, because there are no obvious sources that would reduce the stiffness of the PZT probe in the water. Moreover, stiffness is inversely proportional to the displacement. Since the displacement has changed from 10 nm/V in air to 22 nm/V in water, it implies a more than 50% reduction of stiffness in the water. There are no known mechanisms causing such a significant stiffness reduction in water in such a short time scale. Therefore, we rule out this possibility.

The second mechanism is that the excitation to the system has increased. According to the impedance measurements in Fig. 19, the capacitance (and thus the dielectric constant) of the PZT diaphragm has increased in the first 2 h. This implies that excitation per unit voltage applied to the PZT diaphragm has increased. But where does the increase of dielectric constant come from?

We hypothesize that water has infiltrated into the PZT thin film. Fig. 20 shows a schematic drawing of the hypothesis. As we know, sol–gel derived PZT thin films tend to be porous. Nano-channels form under the porous PZT surface as a result of the sol–gel processes. When the top electrode is deposited at a pressure around 3×10^{-6} torr, the deposition is unidirectional. Therefore, only the area directly facing the pores is covered with the top electrode. In contrast, the parylene molecules, deposited at a pressure of 0.1 torr, have a much smaller mean free path in the deposition chamber; therefore, the parylene coating is omni-directional. Therefore, all interior surfaces will be coated with parylene, and the presence of parylene successfully insulates the top electrodes from the water. When the PZT probe is tested in air, the nano-channels are filled with air (dielectric constant ≈1) resulting in a low dielectric constant of the PZT thin film (about 270). When the PZT probe is tested in water, the nano-channels are filled with water (dielectric constant ≈80), thus increasing the dielectric constant of the PZT thin film resulting in larger excitation to and displacement of the PZT diaphragm.

To support the hypothesis, we have taken SEM image using a 200,000× magnification; see Fig. 21. The images on the left (200,000× and 40,000×) are taken immediately after the PZT thin film is deposited. The images on the right (200,000× and 40,000×) are taken immediately after the top electrodes are deposited onto the PZT thin film. All the SEM images show numerous pores on the surface allowing water molecules to infiltrate.

6. Conclusions

In this paper, we have successfully designed, fabricated, and tested a PZT thin-film microactuator probe that can be potentially implanted in cochlea for animal trials. For the design phase of the PZT probes, the finite element simulations show that reduction of actuator displacement due to the parylene package is less than 3% if the thickness of parylene is 0.25 μm. The back-of-the-envelope calculation ensures that the actuator bandwidth exceeds the audible frequency range when the implantation length is less than 5.9 mm. For the fabrication phase of the PZT probes, the radial mask layouts turn out to be very effective. Using DRIE as a release mechanism to dice the fabricated PZT probes off the wafer is a success. Use of a holder fixture proves to be important when handling the PZT probes before, during, and after the parylene deposition. For the testing phase of the research, it proves to be critical to have both LDV and impedance measurements in order to understand the complicated physics associated with the PZT probes. When submerged in water, the tested PZT probe functions normally for 55 h without failure, indicating that the parylene package is indeed functional. Moreover, the PZT probe increases its displacement in the first 2 h as a result of an increase of its dielectric constant. This phenomenon can be well supported via a hypothesis that water molecules have infiltrated into the PZT thin film due to nano-pores on the film surface as a result of sol–gel processes.

Acknowledgments

This material is based upon work supported by the National Science Foundation under Grant No. CBET-1159623. Any opinions, findings, and conclusions or recommendations expressed in this material are those of the authors and do not necessarily reflect the views of the National Science Foundation.

References

[1] B.J. Gantz, C. Turner, K.E. Gfeller, M.W. Lowder, Preservation of hearing in cochlear implant surgery: advantages of combined electrical and acoustical speech processing, The Laryngoscope 115 (2005) 796–802.
[2] B.S. Wilson, D.T. Lawson, J.M. Muller, R.S. Tyler, J. Kiefer, Cochlear implants: some likely next steps, Annual Review of Biomedical Engineering 5 (2003) 207–249.
[3] M.F. Dorman, R.H. Gifford, Combining acoustic and electric stimulation in the service of speech recognition, International Journal of Audiology 49 (2010) 912–919.

[4] C.C. Lee, C.R. Hume, G.Z. Cao, I.Y. Shen, Development of PZT thin-film microactuators for hybrid cochlear implants, in: Abstracts of 2005 Conference on Implantable Auditory Prostheses, Asilomar, CA, USA, August 1–4, 2005.
[5] C.C. Lee, C.R. Hume, G.Z. Cao, I.Y. Shen, A feasibility study of PZT thin-film microactuators for hybrid cochlear implants, in: Proceedings of 27th Annual International Conference of the IEEE Engineering in Medicine and Biology Society, Paper #1034, Shanghai, China, September 1–4, 2005.
[6] C.C. Lee, Q. Guo, G.Z. Cao, I.Y. Shen, Effect of electrode size and silicon residue on piezoelectric membrane actuators, Sensors and Actuators A-Physical 147 (2008) 279–285.
[7] C.C. Lee, C.R. Hume, G.Z. Cao, I.Y. Shen, Temporary packaging of PZT thin-film microactuators, Integrated Ferroelectrics 101 (2009) 121–131.
[8] C.-C. Lee, G.Z. Cao, I.Y. Shen, Effects of residual stresses on lead–zirconate–titanate (PZT) thin-film membrane microactuators, Sensors and Actuators A—Physical 159 (2010) 88–95.
[9] G.Z. Chuan Luo, I.Y. Cao, Shen, Enhancing displacement of lead-zirconate-titanate (PZT) thin-film membrane microactuators via a dual electrode design, Sensors and Actuators A—Physical 173 (2012) 190–196.
[10] Y. Choe, L. Wang, et al., On-chip integration of eight directional droplet ejectors for inking a spot with eight droplets without ejector movement, in: International Solid-State Sensors, Actuators and Microsystems Conference, 2011.
[11] M. Kagerer, D. Rumschoettel, et al., Fabrication and application of a chemical resistant low-cost microdrop generator, in: International Mechanical Engineering Congress and Exposition, IMECE, 2011.
[12] Y. Luo, M. Lu, et al., A polymer-based bidirectional micropump driven by a PZT bimorph, Microsystem Technologies 17 (3) (2011) 403–409.
[13] H.-K. Ma, J.-S. Wang, et al., The performance of a novel pseudo-bipolar bi-cell piezoelectric proton exchange membrane fuel cell with a smaller nozzle and diffuser, Journal of Power Sources 196 (18) (2011) 7564–7571.
[14] E. Sayar, B. Farouk, Multifield analysis of a piezoelectric valveless micropump: Effects of actuation frequency and electric potential, Smart Materials and Structures 21 (7) (2012).
[15] U. Baran, D. Brown, et al., Resonant PZT MEMS scanner for high-resolution displays, Journal of Microelectromechanical Systems 21 (6) (2012) 1303–1310.
[16] K.H. Gilchrist, D.E. Dausch, et al., Electromechanical performance of piezoelectric scanning mirrors for medical endoscopy, Sensors and Actuators, A: Physical 178 (2012) 193–201.
[17] K.H. Koh, T. Kobayashi, et al., Novel piezoelectric actuation mechanism for a gimbal-less mirror in 2D raster scanning applications, Journal of Micromechanics and Microengineering 21 (7) (2011).
[18] S. Matsushita, I. Kanno, et al., Metal-based piezoelectric microelectromechanical systems scanner composed of Pb(Zr, Ti)O3 thin film on titanium substrate, Microsystem Technologies 18 (6) (2012) 765–771.
[19] S. Yuana, W. Liu, et al., Analysis and test of an optical scanner actuated by PZT films, in: 6th China International Conference on High-Performance Ceramics, CICC-6, August, 2009.
[20] E.-H. Yang, Y. Hishinuma, et al., Thin-film piezoelectric unimorph actuator-based deformable mirror with a transferred silicon membrane, Journal of Microelectromechanical Systems 15 (5) (2006) 1214–1225.
[21] M.A. Matin, D. Akai, et al., Characterization of the deflection of a new epitaxial piezoelectric micro-mirror: modeling and experiment, Materials Science and Engineering B: Solid-State Materials for Advanced Technology 175 (2) (2010) 129–135.
[22] M. Sato, S. Tsuda, et al., Development of piezoelectric MEMS deformable mirror, Springer Verlag, Heidelberg, Germany, 2010, Tiergartenstrasse 17, D-69121.
[23] Y. Choe, S. Chen, E.S. Kim, High fidelity loud microspeaker based on PZT bimorph diaphragm, in: NSTI Nanotechnology Conference and Expo, February, 2010, pp. 316–319.
[24] J. Cho, S. Jang, H. Nam, A piezoelectrically actuated mems speaker with polyimide membrane and thin film pb(zr ti)o3(pzt) actuator, Integrated Ferroelectrics 105 (2) (2009) 7–36.
[25] X. Ting, M. Jianmin, et al., Investigation of the effect of adsorption induced surface stress on the resonant frequency of PZT membrane based biosensors, in: 2010 5th IEEE International Conference on Nano/Micro Engineered and Molecular Systems (NEMS 2010), 20–23, January, 2010.
[26] S. Li, W. Ren, et al., Ferroelectric thin film diaphragm resonators for bio-detection, in: 12th International Meeting on Ferroelectricity, IMF-12 and the 18th IEEE International Symposium on Applications of Ferroelectrics, ISAF-18, August, 2009.
[27] D.F. Wang, X. Li, et al., Ring-shaped PZT film resonator for bio-sensing applications in liquid environment, in: 25th Eurosensors Conference, September, 2011.
[28] I.O.M. Kanja, et al., High sensitivity ultrasonic transducer array for 2-D hydrop0hone application, using an epitaxial PZT thin film grown on -Al 2O3/Si, in: 15th International Conference on Solid-State Sensors, Actuators and Microsystems, June, 2009.
[29] G.L. Smith, R.Q. Rudy, et al., Integrated thin-film piezoelectric traveling wave ultrasonic motors, in: 16th International Solid-State Sensors. Actuators and Microsystems Conference, June, 2011.
[30] I. Ahmed, D. Halupka, et al., A 3-axis PZT-based MEMS gyroscope in 0.18 m CMOS, in: 38th European Solid State Circuits Conference, ESSCIRC, September, 2012.
[31] E. Fuentes-Fernandez, L. Baldenegro-Perez, Optimization of Pb(Zr0.53,Ti0.47)O3 films for micropower generation using integrated cantilevers, Solid-State Electronics 63 (1) (2011) 89–93.
[32] I. Kuehne, M. Schreiter, et al., A novel MEMS design of a piezoelectric generator for fluid-actuated energy conversion, in: Smart Sensors, Actuators, and MEMS V, April, 2011.
[33] I. Kanno, T. Ichida, et al., Power-generation performance of lead-free (K,Na)NbO3 piezoelectric thin-film energy harvesters, Sensors and Actuators, A 179 (2012) 132–136.
[34] S. Kimura, S. Tomioka, et al., Improved performances of acoustic energy harvester fabricated using sol/gel lead zirconate titanate thin film, Japanese Journal of Applied Physics 50 (6 (Part 2)) (2011).
[35] K. Wasa, T. Matsushima, et al., Thin-film piezoelectric materials for a better energy harvesting MEMS, Journal of Microelectromechanical Systems 21 (2) (2012) 451–457.
[36] D. Isarakorn, D. Briand, et al., Finite element analysis and experiments on a silicon membrane actuated by an epitaxial PZT thin film for localized-mass sensing applications, Sensors and Actuators, B 153 (1) (2011) 54–63.
[37] D.G. Hwang, Y.M. Chae, et al., Fabrication and characterization of PZT (lead zirconate titanate) bridge-shaped resonator for mass sensing application, Journal of Electroceramics 29 (3) (2012) 225–234.
[38] M. Olfatnia, T. Xu, et al., Piezoelectric circular microdiaphragm based pressure sensors, Sensors and Actuators, A 163 (1) (2010) 32–36.
[39] E. Heinonen, J. Juuti, et al., High performance thin film PZT ultrasonic transducer by CSD for distance measurements in water, Journal of Electroceramics 27 (1) (2011) 24–28.